Solid Solubility and Transport Properties of Nanocrystalline$(CeO_2)_{1-x}(BiO_{1.5})_x$ by Hydrothermal Conditions

Guangshe Li,*,†,‡ Yachun Mao,† Liping Li,§ Shouhua Feng,† Minqiang Wang,‡ and Xi Yao‡

Key Laboratory of Inorganic Synthesis and Preparative Chemistry, Jilin University, 130023 Changchun, People's Republic of China, Electronic Materials Research Laboratory, Xi'an Jiaotong University, 710049 Xi'an, People's Republic of China, Department of Physics, Jilin University, 130023 Changchun, People's Republic of China

Received September 24, 1998. Revised Manuscript Received January 22, 1999

A series of nanocrystalline solid solutions $(CeO_2)_{1-x}(BiO_{1.5})_x$ ($x = 0.0-0.5$) were synthesized by mild hydrothermal conditions at 240 °C. The products were characterized by X-ray diffraction (XRD), scanning electronic microscope (SEM), X-ray photoelectron spectroscopy (XPS), and electron paramagnetic resonance (EPR). Different from the solid-state reaction systems, the solution limit of Bi_2O_3 in ceria by hydrothermal conditions was as high as ca. 50%. XRD data showed that all solid solutions crystallized in single-phase cubic fluorite-type structure. The average grain size of all solid solutions was within nanometer scale. XPS data gave evidence of the presence of Bi(III) and Ce(IV) on the surface of the doped ceria. EPR measurements confirmed Ce(III) ions in the bulk of the sintered solutions. When the content of dopant Bi_2O_3 in ceria was lower than the limit, air firing of the as-made doped ceria up to 800 °C did not lead to any structural transformation. For the solution $(CeO_2)_{0.5}$-$(BiO_{1.5})_{0.5}$, however, sintering it in air at 800 °C would destabilize the cubic fluorite structure and result in segregation of an unknown phase. The ionic conduction measured by impedance spectroscopy showed that the solid solutions with dopant content lower than the limit exhibited primarily the bulk conduction, whereas for the sintered $(CeO_2)_{0.5}(BiO_{1.5})_{0.5}$, both the bulk and grain boundary resistance decreased dramatically with increasing temperature when using silver electrode. The solution $(CeO_2)_{0.6}(BiO_{1.5})_{0.4}$ was determined to be the best conducting phase. For the nanocrystalline solutions $(CeO_2)_{1-x}(BiO_{1.5})_x$, the bulk conduction was due to oxide ions. The variations of the activation energy and conductivity with dopant content were interpreted in terms of the relative content of the dopant−defect complexes, $Ce_{Ce}'V\ddot{o}/Bi_{Ce}'V\ddot{o}$.

Introduction

Defect chemistry represents an interesting research area because its study can provide an understanding of the remarkable physicochemical properties of defect solids and allows exploration of novel materials. δ-Bi_2O_3 crystallizes in a defect fluorite structure with 25% of the oxide ion sites unoccupied. Its excellent oxide ion conductivity is well-known, but the related fcc cubic structure is stable only between 730 and 825 °C, which restricts to some degree its application as an electrolyte for fuel cells.[1−3] With regard to the formation of low-temperature, high-conductivity oxide ion conductors, stabilization of the high-temperature form, δ-Bi_2O_3, has attracted extensive attention. One of the most effective methods for this goal is doping various oxides. A typical example is isovalent substitution, for example, lanthanide sesquioxide. When Bi_2O_3 is doped with different percentages of Ln_2O_3 (Ln = La−Er and Y),[4−7] various low-temperature phases are formed. With increasing temperature, all these low-temperature phases change into the high-temperature stable δ-phase. It was considered that the Ln_2O_3 stabilized δ-phase was a quenched high-temperature phase but was metastable at low temperatures. Aliovalent substitution can also stabilize the δ-phases; for example, double simultaneous substitution of bismuth also yields high conductivity.[8,9] Among the four polymorphic forms of Bi_2O_3,[10] Roth and Harwig[11] suggested that the high-temperature cubic phase

* To whom correspondence should be addressed. E-mail: guangshe@hotmail.com.
† Key Laboratory of Inorganic Synthesis and Preparative Chemistry, Jilin University.
‡ Xi'an Jiaotong University.
§ Department of Physics, Jilin University.

(1) Kudo, K. T.; Fucki, K. *Solid State Ionics*; VCH: New York, 1990.
(2) Azad, A. M.; Larose, S.; Akbar, S. A. *J. Mater. Sci.* **1994**, *29*, 4135.
(3) Takahashi, T.; Iwahara, H.; Arao, T. *J. Appl. Electrochem.* **1975**, *5*, 187.
(4) Conflant, P.; Follet-Houttemane, C.; Drache, M. *J. Mater. Chem.* **1991**, *1*, 649.
(5) Watanabe, A.; Drache, M.; Wignacourt, J. P.; Conflant, P.; Boivin, J. C. *Solid State Ionics* **1993**, *67*, 25.
(6) Watanabe, A. *J. Solid State Chem.* **1995**, *120*, 32.
(7) Watanabe, A. *J. Solid State Chem.* **1996**, *124*, 287.
(8) (a) Amarilla, J. M.; Rojas, R. M. *Chem. Mater.* **1996**, *8*, 401. (b) Amarilla, J. M.; Rojas, R. M.; Herrero, M. P. *Chem. Mater.* **1995**, *7*, 341.
(9) Laroussi, B.; Khairoun, S.; Tressaud, A.; Reau, J. M. *J. Alloys Compd.* **1993**, *200*, 19.

10.1021/cm9806735 CCC: $18.00
Published on Web 04/24/1999

(δ-Bi_2O_3) and low-temperature monoclinic structure (α-Bi_2O_3) were thermodynamically stable, whereas the tetragonal (β-Bi_2O_3) and body center cubic (γ-Bi_2O_3) were metastable. Some ambiguities still exist about the structural stabilities of the δ-phases.[12]

In the lanthanide series, cerium is a typical element with valence variations. Compounds containing cerium ions always exhibit novel structures and properties. CeO_2 has a prototype fluorite structure and usually acts as a *n*-type conductor.[13] As known, the oxides with this structure can readily incorporate aliovalent ions by forming charge-compensating defects on the oxygen sublattice, that is, oxygen vacancies as well as interstitial defects due to the acceptor/donor doping. On this account, ceria-based solid solutions formed by doping lower valence ions, such as the alkaline earths, possess oxide ion conductivity higher than yittium-stabilized zirconia (YSZ).[14−16] On the other hand, rich conduction behaviors have been found in doped ceria. The solid solution of $(CeO_2)_{1-x}(SrO)_x$ is an important example. When $x = 0.5$, the perovskite $SrCeO_3$, thus formed, is a protonic conductor.[17]

Both δ-Bi_2O_3 and CeO_2 crystallize in the fluorite structure, the former having a considerably larger unit cell size,[18] that is, $a = 0.5411$ nm for CeO_2, while it is 0.5660 nm for Bi_2O_3. Though there exist some structural misfits because of the differences in ionic size and valence state, the structural similarity between these oxides favors mutual solubility by cation diffusion. There might exist a large solubility of Bi_2O_3 in CeO_2 by enlarging the cell volume and retaining cubic symmetry. Alternatively, the stabilization of δ-Bi_2O_3 as well as the formation of Bi-based solid solutions at room temperature might be accomplished using CeO_2 as a stabilizer. Hund[19] reported solid solutions of Bi_2O_3−CeO_2 with 0−40 mol % Bi_2O_3 dopant. Recently, however, Chen and Eysel[20] disclaimed the solution relationship between Bi_2O_3−CeO_2 and showed that CeO_2 could stabilize β-Bi_2O_3 by forming a mixture.

It should be noted that most of the above-mentioned reactions were performed through solid-state reaction routes. It is of great interest to synthesize these materials by mild hydrothermal conditions because of the possible solubility between CeO_2 and Bi_2O_3 and the preference of forming metastable as well as nanocrystalline solids. Previous work on hydrogarnets showed that hydrothermal crystallization has some advantages, for example, reaction homogeneity and low-temperature crystallization in the formation of nanocrystals and defect solids.[21] In the present work, we extend our research toward the possible solid solution relationship in Bi_2O_3−CeO_2 hydrothermal systems and examine the structural stabilities, defect characteristics, and transport properties of the resulting products, on the basis of our previous study on the structural stabilities and valence characteristics of cerium hydrothermal systems.[22]

Experimental Section

All polycrystalline samples were prepared by mild hydrothermal syntheses. The chemicals, $Ce(NO_3)_3{\cdot}6H_2O$ (analytical reagent) and $Bi(NO_3)_3{\cdot}5H_2O$ (analytical reagent) were used as the starting materials. NaOH was employed as the mineralizer. The typical synthetic procedure was as follows: the bismuth and cerium reagents were first dissolved into some amount of deionized water to form a solution, to which 3 M NaOH solution was added dropwise with magnetic stirring to adjust the pH. With increasing pH of the solution up to 13−14, the suspensions became dark yellowish. The initial molar ratios of the input species were kept in the range 3.0−4.0:0.5:0.45−9.0:600/NaOH: Bi_2O_3:CeO_2:H_2O. The reaction mixtures were then sealed into 14 mL Teflon-lined stainless steel autoclaves and crystallized at 240 °C for 3 days. After the autoclaves were cooled and depressurized, the final products were washed with deionized water until a pH of 7 was reached and dried at room temperature.

The structures of all solid solutions were identified by means of powder X-ray diffraction (XRD) on a Rigaku, D/max-γA, 12 kW XRD diffractometer with a rotating target and Ni-filtered Cu Kα radiation at room temperature. The scan rate was 0.3° 2θ/min. Silicon powder (99.99%) was used as the standard for peak position determination. The lattice parameters for the samples were refined by least-squares methods. The average grain sizes (D) were measured from the XRD peaks using the Scherrer formula: $D = 0.9\lambda/\beta \cos \theta$ (where λ is the X-ray wavelength employed, θ is the diffraction angle of the most intense peak (111), and β is defined as $\beta^2 = \beta m^2 - \beta s^2$, βm is the experimental halfwidth (fwhm) and βs is the fwhm of a standard silicon sample)). The elemental analyses for the samples were carried out on a JEOL JEM 2000-FX scanning electron microscope equipped with an energy-dispersive X-ray spectrometer (EDX) analyzer.

The powder samples were pelletized under a pressure of 40 MPa and calcinated at 800 °C in air for 4 h. This sintering temperature was selected by taking into account the relatively low melting point of Bi_2O_3, that is, 825 °C. The densities of all samples measured by Archimedes method were greater than 90% of the theoretical values, reflecting good sinterability of the resulting solids. The surface morphologies of the pellets were examined by scanning electron microscope (SEM, JEOL JEM 2000-FX). The opposite sides of the pellets were coated with silver or platinum paste and heated at 550 or 800 °C in air for half an hour so as to decompose completely the organic components in the paste. The ionic conductivities of the samples were measured using alternating current impedance spectroscopy (Hewlett-Packard HP4192-LF) with the alternating current having a frequency between 5 Hz and 13 MHz at an amplitude of 50 mV in the temperature range of 200−550 °C in air. The transport characteristics of the solid solutions were determined by conducting the measurements in a mixture of O_2/N_2 for a range of oxygen partial pressures from 0 to 10^5 Pa. During the measurements, the samples were held at the desired temperature and atmosphere until the conductivity stabilized.

(10) (a) Gattew, G. *Z. Anorg. Allg. Chem*. **1959**, *298*, 64. (b) Gattow, G.; Fricke, H. F. *Naturewissenschaften* **1961**, *48*, 620. (c) Gattew, G.; Scrode, H. *Z. Anorg. Allg. Chem*. **1962**, *318*, 176.
(11) (a) Levin, E. M.; Roth, R. S. *J. Res. Natl. Bur. Std*. **1964**, *A68*, 189. (b) 197. (c) Harwig, H. A. *Z. Anorg. Allg. Chem*. **1978**, *444*, 151.
(12) Watanabe, A. *Solid State Ionics* **1990**, *40−41*, 889.
(13) Blumental, R. N.; Brugner, F. S.; Garner, J. E. *J. Electrochem. Soc*. **1973**, *120*, 1230. (b) Panhans, M. A.; Blumenthal, R. N. *Solid State Ionics* **1993**, *60*, 279.
(14) Yahiro, H.; Eguchi, K.; Arai, H. *Solid State Ionics* **1986**, *21*, 37.
(15) Arai, H.; Kunisaki, T.; Shimizu, Y.; Seiyama, T. *Solid State Ionics* **1986**, *20*, 241.
(16) Eguchi, K.; Setoguchi, T.; Inoue, T.; Arai, T. *Solid State Ionics* **1992**, *52*, 165.
(17) Mitsui, A.; Miyayama, M.; Yanagida, H. *Solid State Ionics* **1987**, *22*, 213.
(18) McLung, W. F., Ed. *Powder Diffraction File: Inorganic Phases*; JCPDS, International Centre for Powder Diffraction Data: Swarthmore, PA, 1989; Card No. 27-52 and 34-394.
(19) Hund, F. *Z. Anorg. Allg. Chem*. **1964**, *333*, 128.
(20) Chen, X. L.; Eysel, W. *J. Solid State Chem*. **1996**, *127*, 128.
(21) Li, G.; Feng, S.; Li, L.; Li, X.; Jin, W. *Chem. Mater*. **1997**, *9*, 2894.
(22) Li, G.; Feng, S.; Li, L. *J. Solid State Chem*. **1996**, *126*, 74.

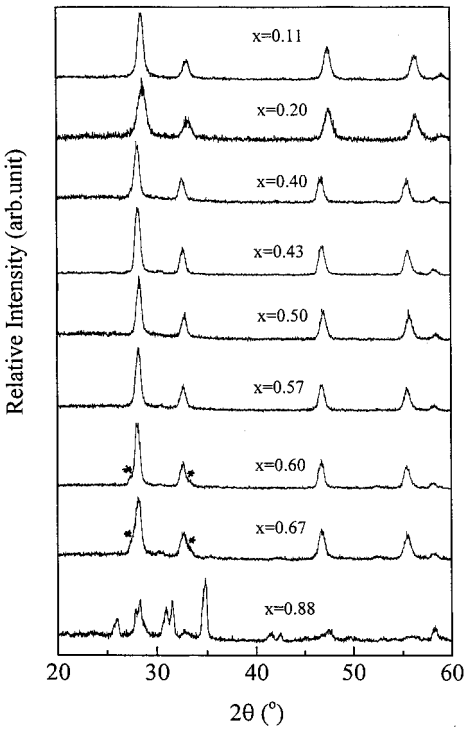

Figure 1. X-ray powder diffraction patterns for the samples $(CeO_2)_{1-x}(BiO_{1.5})_x$ obtained directly by hydrothermal conditions at 240 °C. Obvious broadening effects indicate the formation of nanocrystals. Asterisk denotes the monoclinic phase α-Bi_2O_3.

The valence states of the bismuth and cerium ions for the samples were determined by X-ray photoelectron spectroscopy (XPS). The XPS for powder samples fixed on double-sided tapes was measured on an ESCA-LAB MKII X-ray photoelectron spectrometer from the VG Co. with Al Kα radiation; the base pressure was 10^{-7} Pa. The C1s signal was used to correct the charge effects.

The electron paramagnetic resonance (EPR) measurements were performed on a BRUKER ER200D spectrometer. A frequency of ca. 9.77 GHz was used for a dual-purpose cavity operation. The magnetic field of 0.32 mT was modulated at 100 kHz. A microwave power of ca. 6.5 mW was employed. Reference signals of Mn^{2+} ions in MgO crystals were used as the standard for the precise effective *g*-factor value. All measurements were carried out at 180 K.

Results and Discussion

1. Solid Solution Limit of Bi_2O_3 in Ceria by Mild Hydrothermal Conditions. Rahaman[23] and Greenblatt[24] had prepared ultrafine ceria and ceria-based solutions by hydrothermal syntheses, where cerium nitrate was employed as the cerium species and strong basic concentration was required. To synthesize the nanocrystalline solid solutions from the present CeO_2–Bi_2O_3 hydrothermal systems, the pH of the reaction solutions is fixed as 13−14 so as to keep a strong basic reaction medium. To avoid the influence from other anionic species on the syntheses, bismuth nitrate is selected as the input bismuth species.

Figure 1 illustrates the powder XRD patterns of $(CeO_2)_{1-x}(BiO_{1.5})_x$ prepared by hydrothermal syntheses. All the diffraction peaks for $x \leq 0.57$ are highly symmetric. All the average grain sizes of the as-prepared particles are within a range of 13−19 nm. Scaling up these XRD patterns, we did not observe any weak diffraction peaks of the component oxides, but several intense ones corresponding to the fluorite structure below $2\theta = 60°$, showing no evidence for the monoclinic phase, α-Bi_2O_3. This result is different from that of the hydrothermal systems with $NaBiO_3$ as the precursor where α-Bi_2O_3 usually appeared as the major phase above 190 °C.[25] To do a comparison with the resulting products by solid-state reactions, it is essential here to determine whether some amount of the *β*-Bi_2O_3 component existed in the hydrothermal doped ceria because of the overlapping of most of the diffraction lines of *β*-Bi_2O_3 and *δ*-Bi_2O_3 under the Scherrer line broadening. As known, tetragonal *β*-Bi_2O_3 ($P42_1c$) has a lowered lattice symmetry in comparison to the cubic *δ*-Bi_2O_3 (space group $Pn3m$), which will produce obvious splitting of the diffraction peaks. Theoretically, the splitting difference between the two lines (222) and (400) in the 2θ range of 46−47° for *β*-Bi_2O_3 is ca. 0.7 °, well beyond the measurement limit of this work, since the fwhm of all the bismuth-doped ceria from the present conditions is ca. 0.4 °. In addition, three strong characteristic lines (203), (421), and (213) for *β*-Bi_2O_3 are not observed at $2\theta \sim 55$ °. It is clear that when the content of the dopant Bi_2O_3 is below 57%, the XRD patterns of all samples can be identified with the standard CeO_2, showing the formation of cubic fluorite-type solid solutions. EDX analyses confirmed that all solid solutions contained bismuth and cerium. At ca. 1.04 keV, no obvious emission peak was observed, indicating that sodium from the initial reagents was not in the solid solutions. Our X-ray maps of the elements indicated good homogeneity of Ce and Bi in these solid solutions; no evidence of amorphous phase Bi_2O_3 was seen at the grain boundaries or on the sample surface. The results of semiquantitative analysis by EDX for these solid solutions are listed in Table 1. The molar ratios of Bi to Ce for the resulting solutions of $(CeO_2)_{1-x}(BiO_{1.5})_x$ are similar to the initial ones.

Table 1. Comparison of the Initial Molar Ratios with the Final Ratios for the Solid Solutions

$(CeO_2)_{1-x}(BiO_{1.5})_x$ by Hydrothermal Conditions

initial molar ratio	final molar ratio[a]	formula for the solid solutions
Bi:Ce = 1.00:6.00	Bi:Ce = 1.00:5.67	$(CeO_2)_{0.86}(BiO_{1.5})_{0.14}$
Bi:Ce = 1.00:5.00	Bi:Ce = 1.00:4.65	$(CeO_2)_{0.83}(BiO_{1.5})_{0.17}$
Bi:Ce = 1.00:1.50	Bi:Ce = 1.00:1.46	$(CeO_2)_{0.60}(BiO_{1.5})_{0.40}$
Bi:Ce = 1.00:1.00	Bi:Ce = 1.00:1.05	$(CeO_2)_{0.50}(BiO_{1.5})_{0.50}$

[a] Denotes the results obtained by EDX analysis.

When the dopant content *x* is larger than 0.60, a stable monoclinic phase, α-Bi_2O_3, segregates as a second phase (see Figure 1). Further increasing the dopant levels up to $x = 0.88$ resulted in the formation of an unknown phase. The segregation of α-Bi_2O_3 may be due to a diffusion process. When the content of the dopant Bi_2O_3 is increased up to the limit of the solid solution, some bismuth ions begin to diffuse from the bulk to the surface of the crystallite and produce a bismuth-enriched layer on the surface of the solid solution. But the number of bismuth ions participating in the diffusion process may be relatively small because of the low

(23) Zhou, Y. C.; Rahaman, M. N. *J. Mater. Res.* **1993**, *8*, 1680.
(24) Huang, W.; Shuk, P.; Greenblatt, M. *Chem. Mater.* **1997**, *9*, 2240.
(25) Kinomura, N.; Kumada, N. *Mater. Res. Bull.* **1995**, *30*, 129.

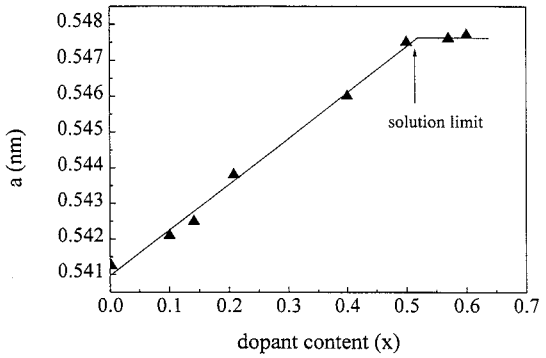

Figure 2. Cubic cell parameter a (nm) vs dopant content x for the solid solutions $(CeO_2)_{1-x}(BiO_{1.5})_x$. The near constant cell parameter for larger x indicates the solution limit of ca. $x = 0.5$.

diffusion rate at a mild crystallization temperature, 240 °C. It is therefore reasonable that the bulk contained bismuth-poor solid solution with the content of Bi_2O_3 lower than the solid solution limit. A similar diffusion process had been found in double substitution of fluorite bismuth oxides.[8b]

The relationship between the lattice parameter and the content x of dopant Bi_2O_3 is shown in Figure 2. The lattice parameter for the undoped ceria is $a = 5.412(1)$ Å, in good agreement with that reported for pure ceria.[18] With increasing Bi_2O_3 content, the lattice parameter for the fluorite solid solutions increases linearly up to $a = 5.477(2)$ Å for $x = 0.50$. It is reasonable that bismuth ions have been incorporated into the CeO_2 lattice by substitution of Ce ions. In the typical cubic fluorite lattice of CeO_2, Ce(IV) cations occupy one-half cube interstitial sites and are coordinated by eight oxygen ions. When Bi(III) ions are incorporated into the Ce(IV) sites, oxygen nonstoichiometry is essential because of charge compensation; that is, with increasing content of the dopant Bi_2O_3, the coordination of the Ce(IV) is lower than 8-fold, and the concentration of the oxygen vacancies (Vö) or/and complex defect associations $\{Bi_{Ce}'Vö\}$ will increase. Additionally, the effective ionic radius of Bi(III) is 1.31 Å and that of Ce(IV) is 1.11 Å with 8-fold coordination.[26] These factors account for the linear increase of the cell parameter with dopant content. As revealed by the XRD patterns in Figure 1, the samples with a dopant content (x) larger than $x = 0.57$ (except for $x = 0.88$) are two-phase mixtures; the predominant phase is still the fluorite structure and the unit cell parameter for the fluorite-type solution is near that of the $x = 0.5$ phase, suggesting that the solution limit of Bi_2O_3 in ceria is ca. 50%.

It is interesting that the solid solutions $(CeO_2)_{1-x}(BiO_{1.5})_x$ can be formed from mild hydrothermal systems and the solution limit reaches up to $x = 0.5$. By contrast, in an analogue of a $CeO_2-Bi_2O_3$ system from a solid-state reaction route,[20] no solid solution could be formed except mixtures. This fact reveals a special solid solubility of Bi_2O_3 in CeO_2 in the present mild hydrothermal systems.

Figure 3 shows the XRD patterns for typical samples obtained by sintering the solid solutions at 800 °C. In comparison to the patterns for the unsintered samples in Figure 1, the peaks of the sintered solutions become

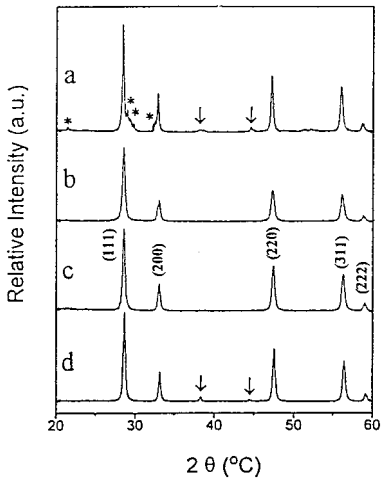

Figure 3. X-ray diffraction patterns for the samples obtained by sintering the nanocrystalline solutions: (a) $(CeO_2)_{0.50}(BiO_{1.5})_{0.50}$, (b) $(CeO_2)_{0.60}(BiO_{1.5})_{0.40}$, (c) $(CeO_2)_{0.83}(Bi_{1.5})_{0.17}$, and (d) $(CeO_2)_{0.86}(BiO_{1.5})_{0.14}$ at 800 °C for half an hour in air. Asterisk corresponds to an unknown phase and the arrowed peaks to the sample holder of aluminum.

slightly narrower. This indicates that upon an increase of temperature of sintering, the grain size grows larger but is still within nanometer scale (<30 nm). All sintered samples with a dopant content (x) lower than 0.5 show the fluorite reflections without new peaks. The intense peaks in Figure 3b−d remain highly symmetric and the relative intensities are similar. Therefore, the cubic fluorite structure is shown to be preserved for lower dopant content. The XRD pattern for the sintered solid solution with 50% Bi_2O_3 doping (see Figure 3a) gives extra peaks, and the peaks do not correspond to any of the component oxides, for example, Bi_2O_3 or CeO_2. This fact suggests that the solid solution with a high Bi_2O_3 content, such as 50% Bi_2O_3, is a low-temperature metastable phase and will decompose into a mixture of a fluorite phase and an unknown phase.

Figure 4 shows several scanning electron micrographs of the pellets obtained after thermal treatments on the as-synthesized solid solutions in air at 800 °C. All pellets exhibit a continuous shape with near-spherical grains and agglomeration phenomena are also obvious. The grain size distributions for these solutions are not uniform and a large amount of fine pores are at the interior of the grains. The abnormal grain growth is in accordance with the mobility disparity among different boundaries, resulting from a nonhomogeneous sintering process.

2. Valence Characteristics of the Nanocrystalline Solid Solutions. The valence state of bismuth ions is measured by XPS. Figure 5a is representative of the Al Kα excited core level spectrum of the nanocrystalline solution $(CeO_2)_{0.6}(BiO_{1.5})_{0.4}$ in the Bi4f region. The signals for Bi4f are typical broad doublets, and both peaks of $Bi4f_{7/2,5/2}$ are highly symmetric, as seen in Figure 5a. The energy positions are at 158.5 eV for $Bi4f_{7/2}$ and 164.1 eV for $Bi4f_{5/2}$. The spin−orbit splitting is therefore 5.6 eV, in good agreement with those observed in the bismuth-stabilized zirconia and bismuth oxide film.[27,28] The bismuth ions in the solid solution were present as Bi(III). After the solid solution was sintered at 800 °C, no peak shift or asymmetry is observed at either the low binding energy or high

(26) Shannon, R. D. *Acta Crystallogr.* **1976**, *A32*, 751.

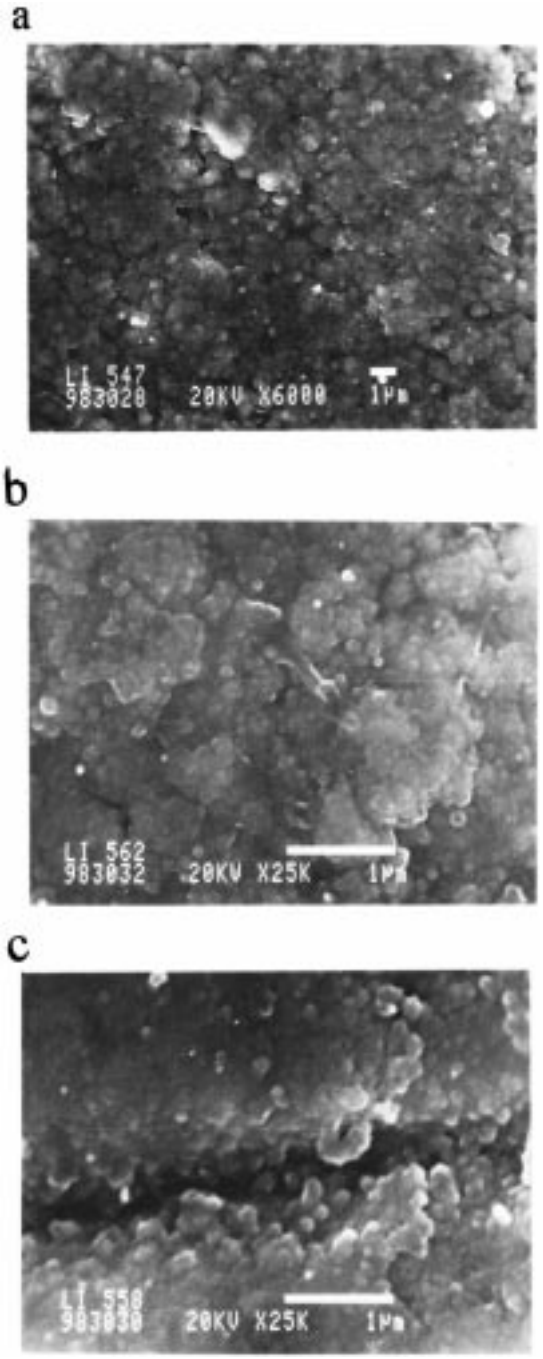

Figure 4. SEM micrographs of the pellets obtained by air sintering of the as-synthesized nanocrystalline solutions: (a) $(CeO_2)_{0.50}(BiO_{1.5})_{0.50}$, (b) $(CeO_2)_{0.60}(BiO_{1.5})_{0.40}$, and (c) $(CeO_2)_{0.83}(Bi_{1.5})_{0.17}$ at 800 °C in air.

binding energy side of the $Bi4f_{7/2,5/2}$ peaks as assigned to the existence of Bi(0) and Bi(V)[29,30] (see Figure 5a). These facts show that Bi(III) is highly stable in the solid solutions as prepared.

Ce(IV) in ceria has a special chemistry feature, that is, its easy reduction to Ce(III) at high temperatures. It has been proposed that, even in pure ceria, there still exists some amount of Ce(III) as well as the corresponding charge-compensating oxygen vacancies (Vö).[31] In the fluorite lattice, Ce(III) and Ce(IV) ions had been shown to interact by exchanging charges via the small polaron mechanism.[32] The core level spectrum of Ce3d for the nanocrystalline $(CeO_2)_{0.6}(BiO_{1.5})_{0.4}$ is shown in Figure 5b. Similar to the undoped ceria obtained directly from the cerium nitrate hydrothermal system,[22] both $Ce3d_{3/2}$ and $Ce3d_{5/2}$ XPSs of the solid solution consist of three peaks; the assignments of the peaks are shown in Figure 5b. Previous studies on Ce3d XPS suggested that the ground state of Ce(IV) was a strongly mixed state between $4f^0$ and $4f^1$ configurations, while three different final states exhibited $4f^0$, $4f^1$, and $4f^2$ configurations arising from the 4f-level relaxation around the core hole,

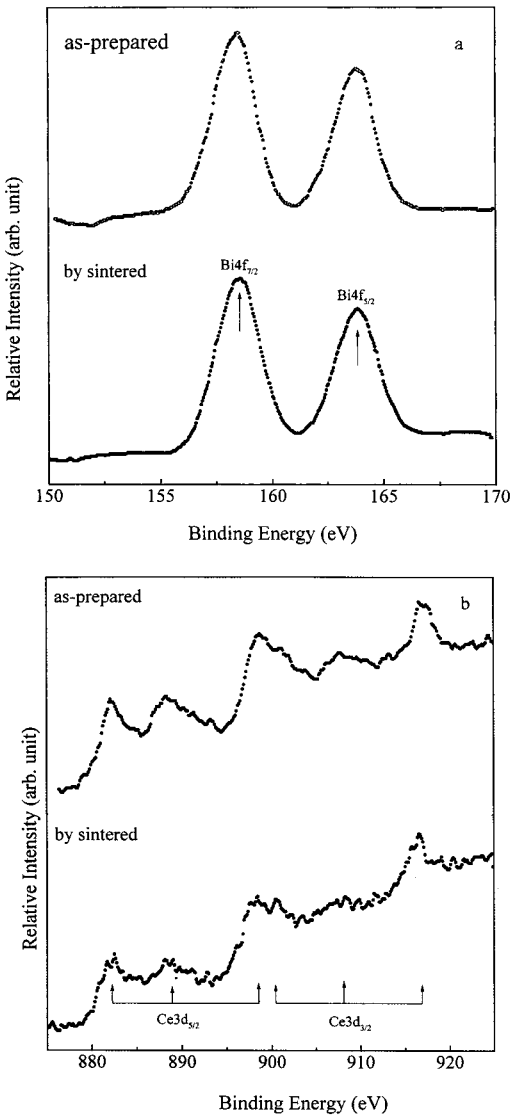

Figure 5. Al Kα excited core level spectra for the nanocrystalline solution $(CeO_2)_{0.60}(BiO_{1.5})_{0.40}$ as synthesized from hydrothermal conditions and by air sintering at 800 °C (a) in a Bi4f binding energy region and (b) in a Ce3d binding energy region. The characteristic broad doublets for Bi4f are high symmetric and the spin−orbit splitting is 5.6 eV, suggesting the presence of Bi(III).

(27) Morgan, W. E.; Stec, W. J.; Van Wazer, J. R. *Inorg. Chem.* **1973**, *12*, 953.
(28) Felthouse, T. R.; Fraundorf, P. B.; Friedman, R. M.; Schosser, C. L. *J. Catal.* **1991**, *127*, 421.
(29) Facer, G. R.; Elcombe, M. M.; Kennedy, B. T. *Aust. J. Chem.* **1993**, *46*, 1897.
(30) Nagoshi, M.; Suzuki, T.; Fukuda, Y.; Tokiwa-Yamamoto, A.; Syono, Y.; Tachiki, M. *Phy. Rev.* **1993**, *47B*, 5196.
(31) Chen, P. L.; Chen, I. W. *J. Am. Ceram. Soc.* **1996**, *79*, 1793 and references therein.
(32) Naik, I. K.; Tien, T. Y. *J. Phys. Chem. Solids* **1978**, *38*, 311.

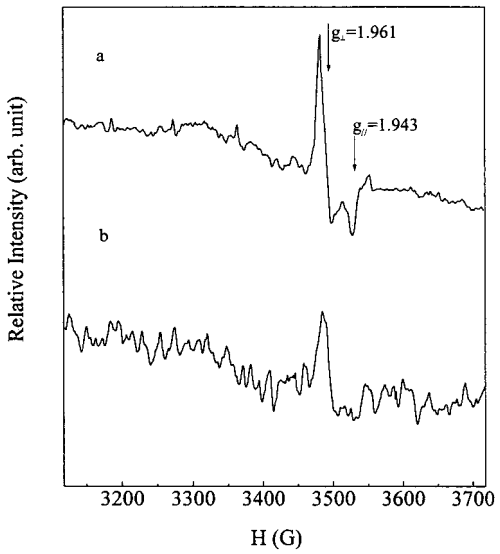

Figure 6. EPR spectra recorded at 180 K for the sintered samples (a) $(CeO_2)_{0.83}(BiO_{1.5})_{0.17}$ and (b) $(CeO_2)_{0.50}(BiO_{1.5})_{0.50}$ sintered at 800 °C in air.

which produced three photoemission peaks,[33] and thus the related binding energy increased in sequence. For the present solid solution $(CeO_2)_{0.6}(BiO_{1.5})_{0.4}$, the main peak position for $Ce3d_{5/2}$ is at 882.2 eV. The adjacent peak appears at ca. 889.0 eV, and its relative shift to the main peak of $Ce3d_{5/2}$ can be used to identify the existence of Ce(III).[34] However, no obvious peak shift is observed for the present solid solution. This gives no indication of Ce(III), which may be due to its content being lower than the instrumental limit. After the solid solution was sintered at 800 °C, as seen in Figure 5b, the peak positions for Ce3d remained near the same as those before sintering. These results confirm the presence of Ce(IV) only on the surface of the sintered solid solutions. In essence, even at higher temperatures than 1200 °C, the relative content of Ce(III) is only ca. 0.2% in the undoped ceria.[31] The characteristic peak at a high binding energy of 916 eV appearing in the Ce3d spectrum is ascribed to Ce(IV).[35] Similar valence characteristics have been found in other as-synthesized solid solutions of $(CeO_2)_{1-x}(BiO_{1.5})_x$. The absence of Ce(III) in our XPS measurements may be ascribed to complete oxidation on the sample surface, promoted by the large surface area of the nanocrystalline solid solutions:

$$O_2 + 4Ce_{Ce}' + 2V\ddot{o} \rightarrow 4Ce_{Ce} + 2Oo \qquad (1)$$

The Ce(III) ions in the bulk of the solid solutions can be determined by EPR measurements, while Ce(IV) and Bi(III) are inactive in EPR for no unpaired electrons. Figure 6 shows the EPR spectra observed at 180 K for the solutions $(CeO_2)_{0.83}(BiO_{1.5})_{0.17}$ and $(CeO_2)_{0.50}(BiO_{1.5})_{0.50}$ sintered in air at 800 °C. As shown in Figure 6a, the spectrum for sintered $(CeO_2)_{0.83}(BiO_{1.5})_{0.17}$ gives the signals of an axial symmetry with $g_\perp = 1.961$ and $g_{||} = 1.943$, the characteristics of Ce(III) ions in the bulk of the solids, as stabilized by the lattice defects.[36] For the sintered $(CeO_2)_{0.50}(BiO_{1.5})_{0.50}$ as shown in Figure 6b, we also observed the signals with the same g-values although the relative intensities are slightly weaker than those of Figure 6a. These results confirm the presence of Ce(III) in the bulk of the sintered solid solutions and the decrease of its relative content with the increment of dopant Bi_2O_3.

3. Transport Properties of the Doped Ceria Solid Solutions. The conductivities for nanocrystalline solid solutions $(CeO_2)_{1-x}(BiO_{1.5})_x$ were determined by the complex impedance technique. It is found that the conductivity increases dramatically with increasing temperature. The impedance plot for the solid solution $(CeO_2)_{0.5}(BiO_{1.5})_{0.5}$ measured at 210 °C using a silver electrode shows only one distinct semicircle at high frequency, which is primarily contributed by the bulk effect,[37] whereas the grain boundary conduction is negligible because of the similar time constants for both bulk and grain boundary impedances. Above 300 °C, as shown in Figure 7, the grain boundary effects become obvious, which is ascribed to an overlapping of the grain boundary process and electrode−electrolyte interphase contribution. On the basis of our SEM observations and impedance measurements, we believe that such grain boundary effects cannot be attributed simply to porosity at the boundaries. Similar conclusions were drawn in other ceria-based solutions.[37] The most striking observation obtained in the present work is the determination that the grain boundary effect can be virtually eliminated when the silver electrode was replaced by a Pt blocking electrode. As shown in Figure 7, only bulk conduction was observed in the case of the Pt electrode with a resistance nearly equal to the bulk component when using an Ag electrode. The beginning of a third relaxation mode is observed at low frequency in Figure 7, reflecting an oxygen exchange process occurring at the electrode−electrolyte interface.[38] For the nanocrystalline solid solutions, a large number of coordination unsaturated atoms exist at the grain boundaries; the large specific surface can lead to the production of lattice defects and the adsorption of oxygen, allowing the development of a high oxygen exchange rate

$$^1/_2O_2\,(gas) + 2e^-\,(electrode) \leftrightarrow O^{2-}\,(electrolyte) \quad (2)$$

at the grain boundary interface and promoting oxygen ion conduction in the bulk. This conduction behavior is slightly different from that of electrolytes based on stabilized bismuth oxides, where no evidence of a grain boundary contribution to the conductivity was shown;[39] the effect of the dopant was just to lower the conductivity.[40]

The conductivities are determined by the intersections of the corresponding semicircles on the real part of the impedance axis. Figure 8 gives $\ln \sigma T$ versus $1/T$ plots for the sintered $(CeO_2)_{0.5}(BiO_{1.5})_{0.5}$. The conductivity data recorded during the first cooling and subsequent heating cycles fall on the same plot, indicating that the experimental data represent the reliable conductivity

(33) Kotani, A.; Jo, T.; Parlebas, J. C. *Adv. Phys.* **1988**, *37*, 38.
(34) Li, L.; Wei, Q.; Liu, H.; Su, W. Z. *Phys. B* **1995**, *96*, 451.
(35) Pralime, G.; Koel, B. E.; Hance, R. L.; Lee, H. L.; White, J. M. *J. Electron Spectrosc. Relat. Phenom.* **1980**, *21*, 17.
(36) Abi-aad, E.; Bechara, R.; Grimblot, J.; Aboukais, A. *Chem. Mater.* **1993**, *5*, 793.
(37) Gerhardt, R.; Nowick, A. S. *J. Am. Ceram. Soc.* **1986**, *69*, 641.
(38) Macdonald, J. R. *Impedance Spectroscopy*; Wiley: New York, 1987.
(39) Jurago, J. R.; Moure, C.; Duran, P. *Solid State Ionics* **1988**, *28−30*, 518.
(40) Takahashi, T.; Iwahara, H. *Mater. Res. Bull.* **1978**, *13*, 1447.

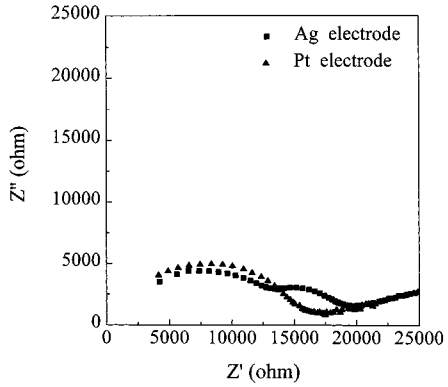

Figure 7. Comparison of the impedance spectra measured at 300 °C for the sintered solid solution $(CeO_2)_{0.50}(BiO_{1.5})_{0.50}$ using different electrodes.

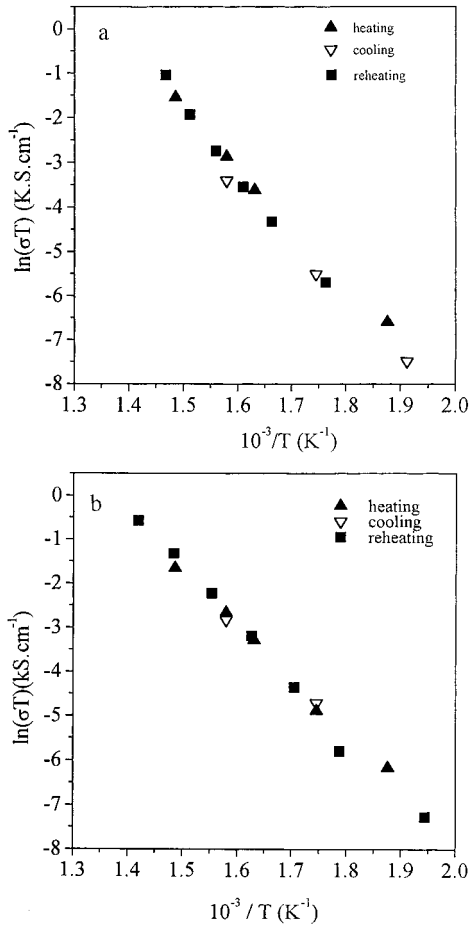

Figure 8. The temperature dependence of (a) the bulk and (b) grain boundary conductivities of the sintered solid solution $(CeO_2)_{0.50}(BiO_{1.5})_{0.50}$ using a silver electrode.

of the solid solution. At 400 °C, the bulk conductivity reaches values as high as ca. 3.8×10^{-4} S/cm, far beyond that for YSZ measured at the same temperature.[41] The conductivity data for the solid solution fall onto two straight lines, showing that the conductivity is by oxide ions, and the conductivity−temperature dependencies for the bulk and overlapping contributions from the grain boundary and electrode−electrolyte interphases exhibit Arrhenius behavior. The activation energy (E_a) obtained from the slope of the experimental data for the

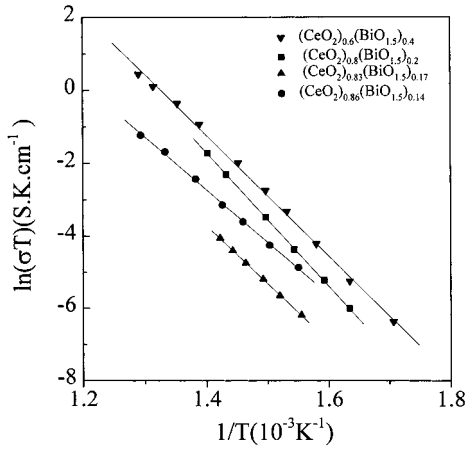

Figure 9. The temperature dependence of the conductivity of the solid solutions having a bismuth content lower than the solution limit, 50 mol % Bi_2O_3 (silver electrode).

Table 2. Activation Energies for the Bulk Conduction in the Nanocrystalline Solid Solutions

$(CeO_2)_{1-x}(BiO_{1.5})_x$		
solid solutions	activation energy (eV)	temperature range (°C)
$(CeO_2)_{0.86}(BiO_{1.5})_{0.14}$	1.25	372−500
$(CeO_2)_{0.83}(BiO_{1.5})_{0.17}$	1.39	339−450
$(CeO_2)_{0.80}(BiO_{1.5})_{0.20}$	1.59	188−350
$(CeO_2)_{0.60}(BiO_{1.5})_{0.40}$	1.44	313−500
$(CeO_2)_{0.50}(BiO_{1.5})_{0.50}$	1.34	210−400

latter part is 1.17 eV, slightly smaller than that for the bulk part, 1.34 eV. Similar activation energies have been reported in the nanocrystalline CeO_{2-x}[42] and Bi_2O_3−Er_2O_3 solutions.[43] The obvious difference between Figure 8a and 8b arises from the bismuth-enriched phases having high conductivity segregated on the surface or at the grain boundaries of the solid solution, as detected by the XRD of Figure 3a. It is noteworthy that the bulk conductivity of the sintered $(CeO_2)_{0.5}(BiO_{1.5})_{0.5}$ is the only contribution which is clearly measurable in the present work. This is because the grain boundary effects involve complex contributions, such as those from the interphases due to the strong reaction between the metallic electrodes and bismuth-containing electrolytes.[43,44] Our XRD did not reveal any evidence of the presence of interphases on the sample surface after the conduction measurements, probably owing to a content below the experimentally detectable limit.

The solid solutions $(CeO_2)_{1-x}(BiO_{1.5})_x$ with bismuth content lower than the solution limit, that is, $x < 0.5$, show primarily bulk conduction despite the fine pores at the interior of the grains (shown in Figure 4). All the conductivity data fall onto straight lines, as seen in Figure 9. The respective activation energy data are listed in Table 2. For comparison, the activation energy of bulk conduction for $x = 0.5$ is also included. For the nanocrystalline solutions $(CeO_2)_x(BiO_{1.5})_x$, the activation energy increases with x up to a maximum at $x = 0.2$. Beyond this range, the activation energy decreases.

(41) Ziehfreund, A.; Simon, U.; Maier, W. F. *Adv. Mater.* **1996**, *8*, 424.

(42) Chiang, Y. M.; Levik, E. B.; Kosacki, I.; Tuller, H. L.; Ying, J. Y. *J. Electroceram.*, **1997**, 1, 7; *Appl. Phys. Lett.* **1996**, *69*, 185.

(43) Duran, P.; Jurado, J. R.; Moure, C.; Valverde, N.; Steele, B. C. N. *Mater. Chem. Phys.* **1996**, *8*, 642.

(44) (a) Pravoverov, N. L.; Afonin, M. P.; Vyatkin, L. V.; Mashkov, N. M.; Tribunskaya, I. A. *Poroshk. Metall.* **1986**, *11*, 20, (b) Tanabe, H.; Fukushima, S. *Nippon Kagaku Kaishi* **1986**, *10*, 1275.

However, the conductivity varies oppositely: a minimum is at $x = 0.17$ and the conductivity is at a maximum for the $x = 0.4$ phase. These results are different from those of $Ce_{1-x}Sm_xO_{2-x/2}$.[24] To understand these results, we should recall not only the defect characteristics of the doped fluorite solid solutions but also the dopant nature. Common to other trivalent acceptor dopants,[31] every two Bi(III) dopants or Ce(III) ions generate only one Vö in the fluorite lattice of the solid solutions $(CeO_2)_{1-x}(BiO_{1.5})_x$. As revealed by our EPR measurements, the Ce(III) content in the solid solutions $(CeO_2)_{1-x}(BiO_{1.5})_x$ decreases with increasing dopant x. At lower Bi_2O_3 content, the defect complexes Ce_{Ce}'Vö dominate the transport property of the solutions. The decrease of Ce(III) content accounts for the decrease of conductivity and the increase of activation energy. Similar results had been found in reduced ceria CeO_{2-x}.[32] For heavy doping of Bi_2O_3 (for example, the concentration of Bi(III) is much larger than that of Ce(III)) the pronounced Bi−O−Bi bindings in the fluorite lattice may induce a decrease of the relative content of dopant−defect association, Bi_{Ce}'Vö. This can help interpret the gradual decrease of activation energy and increase of conductivity. The variation of the relative content for the complexes, Ce_{Ce}'Vö/ Bi_{Ce}'Vö at intermediate doping x may result in the maximum of activation energy at $x = 0.2$ and the minimum of conductivity at $x = 0.17$.

The relationships between the bulk conductivity of nanocrystalline $(CeO_2)_{1-x}(BiO_{1.5})_x$ and the oxygen partial pressure P_{O_2} were measured at 300 °C. In the oxygen partial pressure range, $0-10^5$ Pa, the bulk conductivity is nearly the same as that obtained in air. The independence of the conductivity on P_{O_2} suggests that the transport mechanism for the bulk of the nanocrystalline solid solutions $(CeO_2)_{1-x}(BiO_{1.5})_x$ is ionic, which is similar to those of other oxide ion conductors.

Conclusions

Nanocrystalline solutions $(CeO_2)_{1-x}(BiO_{1.5})_x$ ($x = 0.0-0.5$) were hydrothermally synthesized at 240 °C. XRD data revealed single-phase cubic fluorite structural characteristics in all solid solutions. The linear dependence of the cell parameters of the solutions on the dopant content of Bi_2O_3 suggested the incorporation of Bi(III) into the fluorite structure by substitution for Ce(IV). XPS data confirmed the presence of Bi(III) and Ce(IV) on the sample surface of all sintered nanocrystals, whereas the bulk contained Ce(III). On sintering up to 800 °C, the metastable solid solutions $(CeO_2)_{1-x}(BiO_{1.5})_x$ with high dopant content (x) formed at low temperature are destabilized; the stability decreases with increasing Bi_2O_3 content. Bulk conductivity exists primarily in the solid solutions with the bismuth content lower than the limit. When the dopant content approaches near the limit, for example, for the doped ceria $(CeO_2)_{0.5}(BiO_{1.5})_{0.5}$, the contributions of the bulk and grain boundary to the total conductivity are successfully isolated by impedance spectroscopy. Both the bulk and grain boundary resistances decrease dramatically on heating the nanocrystalline-doped ceria.

Acknowledgment. This project was financially supported by the China Postdoctoral Foundation (G.L.), NSFC (NO. 19804005), and by a key project on Soft Chemistry Synthesis and the National Outstanding Youth Science Fund (S.F.). G. L. thanks Dr. Linbing Kong for XRD experiment assistance and Sanhong Wang for recording the impedance spectra.

CM9806735